Solution-processable phosphorescent to organic light-emitting diodes based on chromophoric amphiphile/silica nanocomposite

2009 Nanotechnology 20 315601

(http://iopscience.iop.org/0957-4484/20/31/315601)

Nanotechnology **20** (2009) 315601 (7pp) doi:10.1088/0957-4484/20/31/315601

Solution-processable phosphorescent to organic light-emitting diodes based on chromophoric amphiphile/silica nanocomposite

Chung-He Yang, Sheng-Hsiung Yang and Chain-Shu Hsu[1]

Department of Applied Chemistry, National Chiao Tung University, 1001 Ta-Hsueh Road, Hsinchu 30010, Taiwan

E-mail: cshsu@mail.nctu.edu.tw

Received 1 March 2009, in final form 27 May 2009
Published 14 July 2009
Online at stacks.iop.org/Nano/20/315601

Abstract

We report the synthesis of a tris-cyclometalated iridium complex which emits sky-blue light and its potential use in phosphorescent light-emitting devices. The hybrid meso-structured nanocomposites by sol–gel co-assembly with tetraethyl *ortho*-silicate and corresponding molecular interactions within mesopores were also demonstrated. Electroluminescent devices were fabricated using carbazole-based monomers and iridium complex as the active layer, acting as a host/guest system through a co-assembled sol–gel process. Devices based on this nanocomposite showed improved luminescent efficiencies several times higher than that of similar chromophores elaborated in the literature. A triple-layer electroluminescence device with the configuration of ITO/PEDOT/Ir(F2OC11ppy)$_3$:CA-C11:PBD nanocomposite/TPBI/Ca/Al showed a maximum brightness of 1389 cd m^{-2} at 12 V and a maximum efficiency of 3.29 cd A^{-1}.

S Supplementary data are available from stacks.iop.org/Nano/20/315601

1. Introduction

Recent developments in the organic-templated growth of materials have given rise to new types of photonic hybrid composites whose structures and functions are organized hierarchically. Self-organized mesostructure can be achieved through the sol–gel process or self-assembly routes that allow the construction of composites for many types of materials, for example, organic molecules or polymers. Such ordered hybrid materials permit the accommodation and integration of elementary functions of each participating species in a small volume in nanoscale.

The sol–gel synthesis of mesoporous silica with functional templates has attracted attention for the fabrication of nanocomposite materials, in contrast with statistical post-loading approaches, which guarantees dense filling of organic functional groups in the silicate channels [1]. Stable, supported films prepared by this method can be processed into porous or composite mesostructures with a variety of potential applications, such as membranes [2], sensors [3], lasers [4–6], waveguides [5] and low dielectric constant (low k) insulators [7, 8]. Amphiphilic molecules or polymers bearing both hydrophilic and hydrophobic parts are the most common materials. In earlier work, we reported chromophoric amphiphile/silica co-assembled nanocomposites with enhanced emission to overcome the problem of solid-state quenching in the development of organic light-emitting devices [9]. The fabrication of thin layers was essential for many technical applications and the molecules showed an ordered structure within these thin films to enhance or even cause certain desired properties [10].

Modern organic light-emitting diodes (OLEDs) offer substantial benefits over conventional cathode ray tubes and liquid crystal displays [11]. The design of highly luminescent inorganic complexes based on phosphorescent dopants has attracted a great deal of interest in the development of

[1] Author to whom any correspondence should be addressed.

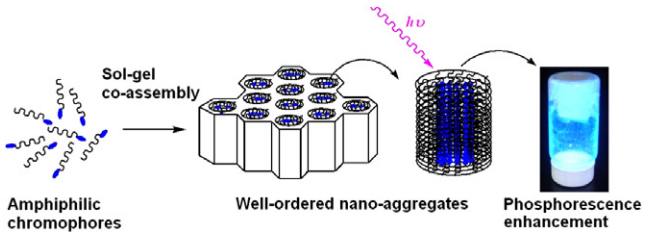

Figure 1. Schematic illustration of hexagonally ordered nanocomposite which shows strong phosphorescence.
(This figure is in colour only in the electronic version)

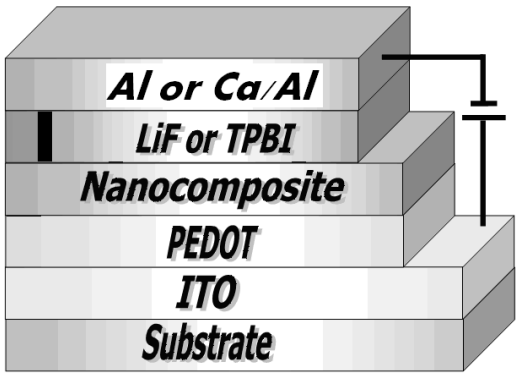

Figure 2. Device structure using nanocomposite as the active layer.

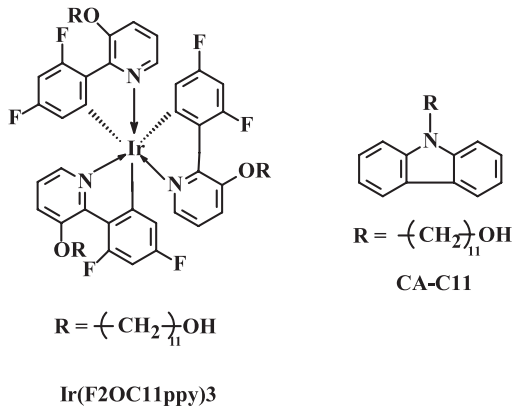

Chart 1. Molecular structures of Ir(F2OC11ppy)$_3$ and CA-C11.

OLEDs [12]. The strong spin–orbit coupling induced by a heavy metal ion such as iridium (III) promotes an efficient intersystem crossing from the singlet to the triplet excited state, which facilitates strong electroluminescence by the harnessing of both singlet and triplet excitons after the initial charge recombination. An internal phosphorescence quantum efficiency (η_{int}) of nearly 100% could theoretically be achieved.

There are several pioneering works on phosphorescent iridium complexes carried out to reach high-efficiency electrophosphorescent devices. First of all, small phosphorescent emitter was co-evaporated with host materials, as well as several extra layers to control charge transport and exciton diffusion [13]. However, this method is limited to low molecular weight molecules with excellent thermal stability, and a huge instrumental expense is required. Secondly, solution-processed light-emitting diodes containing phosphorescent dopants were also proposed [14]. Thin films comprised of complex mixtures, including phosphorescent molecule, polymer host and charge transport materials, were prepared. Despite facile film processing, the luminescent efficiency of these devices is relatively low. Thirdly, tris-cyclometalated iridium complexes with attached carbazole or fluorene units [15] and phenylcarbazole dendrons [16] were synthesized to achieve a host-free approach in solution-processing electrophosphorescent devices. Moreover, dendrimers consist of emissive cores to which one or more branching dendrons are attached; however, complicated synthetic steps and overall low yield are usually a concern [17].

In this study, we demonstrate a novel solution-processable approach to high-efficiency phosphorescent OLEDs. The idea derives from confining phosphorescent chromophores into a mesoporous nanostructure by sol–gel and solvent evaporation-induced self-assembly (EISA) processes [18], as shown in figure 1. The synthesis of a phosphorescent Ir(III) complex [19] with hydrophilic side-arms was reported with good yield. Figure 2 shows the configuration of an organic light-emitting device which is fabricated using the nanocomposite formed as an active layer, consisting of sol–gel co-assembly of silica, Ir(III) complex and a carbazole-based monomer to act as the host/guest system. Furthermore, this approach allows simple fabrication of OLED devices via a spin-coating process. To the best of our knowledge, this is the first report that describes the use of a carbazole-based monomer as host material and a new approach to phosphorescent light-emitting devices by the sol–gel process. The idea and experimental results demonstrated here provide a new way to fabricate high-efficiency light-emitting diodes from an academic viewpoint to industrial production.

2. Experimental details

Chart 1 shows the chemical structures of Ir(III) complex Ir(F2OC11ppy)$_3$ and host material CA-C11. Ir(F2OC11ppy)$_3$ consists of three fluoro-substituted phenylpyridinyl groups as the hydrophobic part and long alkyl chains with hydroxy groups as the hydrophilic part. Detailed synthesis and characterization of these two compounds were depicted in supporting information. The designed Ir(III) complex is a sky-blue light-emitting material with a high photoluminescence (PL) efficiency. In dilute THF solution, the PL external quantum efficiency of Ir(F2OC11ppy)$_3$ was measured to be 62% using an integrating sphere. A hybrid nanocomposite of this phosphorescent amphiphile with silica precursors was formed by sol–gel co-assembly. Precursor solutions were prepared from tetraethyl orthosilicate (TEOS, $Si(OC_2H_5)_4$), phosphorescent amphiphile [Ir(F2OC11ppy)$_3$] and HCl catalyst in THF/H_2O. The mole ratio of reactants in the nanocomposites was set to be TEOS:THF:H_2O:HCl: Ir(F2OC11ppy)$_3$ = 1:30:5:0.1:3. In a typical preparation, TEOS, THF, water and dilute HCl were heated and stirred at 35 °C for half an hour. To this solution was added the phosphorescent amphiphile Ir(F2OC11ppy)$_3$ in THF and stirred for an additional 3 h. The forming colloidal solution

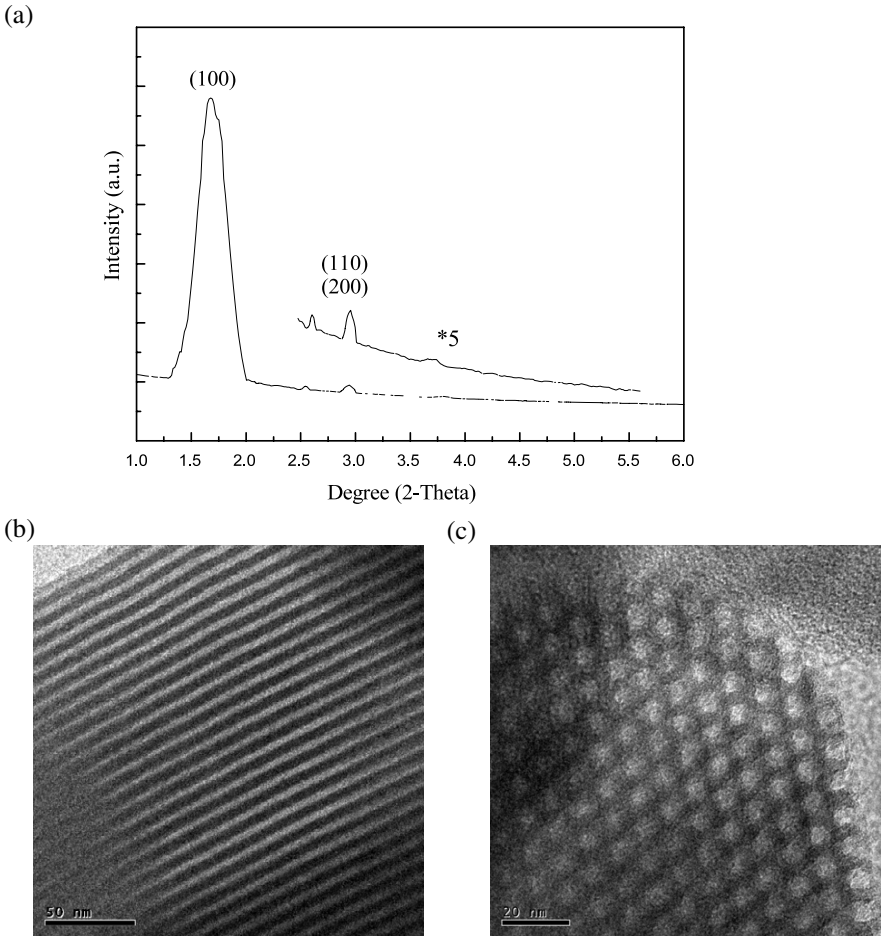

Figure 3. (a) X-ray diffraction (XRD) patterns of nanocomposite thin films formed by Ir(F2OC11ppy)$_3$ and silica. The film shows a hexagonal mesophase with strong (100), (110) and (200) diffraction peaks at 60, 34 and 30 Å, respectively; (b) and (c) TEM micrographs of Ir(F2OC11ppy)$_3$ nanocomposite thin film shows [110]-and [001]-oriented hexagonally ordered structure, respectively.

was then spin-cast into thin films on adequate substrates. Co-assembly of phosphorescent amphiphile/silica mixtures led them to organize into ordered mesophases in the thin film state.

3. Results and discussions

3.1. Spectroscopic properties of the nanocomposite

Figure 3(a) shows the x-ray diffraction (XRD) pattern of the Ir(F2OC11ppy)$_3$/silica nanocomposite thin film. Three individual peaks located at 1.6° (100), 2.6° (110) and 2.9° (200) are observed. The d spacing associated with three diffraction peaks are calculated to be 60, 34, and 30 Å, respectively. These Bragg peaks at the low 2θ region indicate hexagonally periodic packing of silicate structures, which is consistent with a theoretically determined ratio of $1{:}1/\sqrt{3}{:}1/2$. Similar observations were reported for the hierarchically structured transparent hybrid materials by *in situ* growth of mesostructured organosilica in a host polymer [20]. Figures 3(b) and (c) show TEM micrographs of the hexagonally ordered nanocomposite film which reveals a uniform pattern and apparent long-range ordering [21] that is consistent with [110]-and [001]-oriented hexagonal mesophases, respectively, with unit cell parameter $a = 70$ Å [21]. From the highly ordered nanocomposite mesostructures observed by TEM, we infer that the surfactant monomers are uniformly organized into precise spatial arrangements.

We further study the optical properties of the Ir(F2OC11ppy)$_3$/silica nanocomposite. Figure 4 shows the UV–vis absorption spectra of Ir(F2OC11ppy)$_3$ in dilute THF solution. A sharp peak at 216 nm and two broad bands between 250 and 380 nm are observed. The sharp absorption peak at 216 nm is assigned as the π–π^* transition of the surrounding ligands. The two broad bands located at 250–300 nm and 310–380 nm are assigned to be spin-allowed metal to ligand charge-transfer (3MLCT) [$d\pi$(Ir) $\rightarrow$ π(F2OC11ppy)] and 1MLCT [$d\pi$(Ir) $\rightarrow$ π(F2OC11ppy)] transitions, respectively. The photoluminescence (PL) spectra of the Ir(F2OC11ppy)$_3$/silica nanocomposite in THF and the thin film state are shown in figure 5. Ir(F2OC11ppy)$_3$ in THF exhibits a bright blue–green emission with the peak maximum at about 503 nm, and this emission curve reveals that the lowest excited states of the complex have a mixed ligand centered (LC) as well as MLCT character. In the thin film state PL spectra showed a maximum emission band at 548 nm and a lowered band at

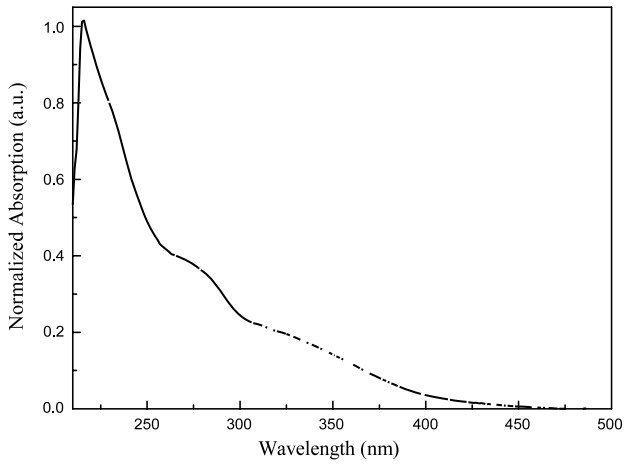

Figure 4. UV–vis absorption spectrum of Ir(F2OC11ppy)$_3$ in dilute THF solution.

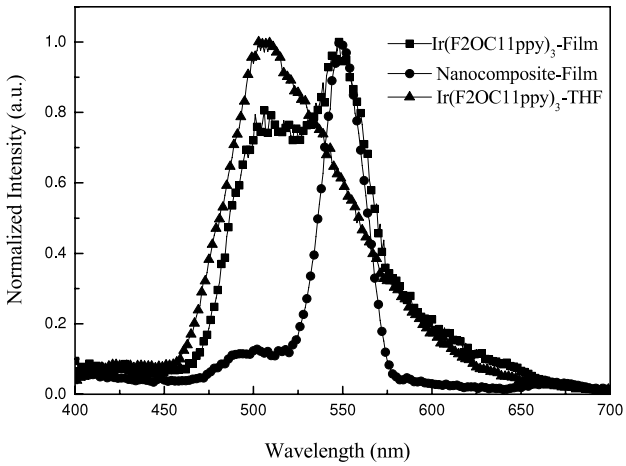

Figure 5. Normalized PL spectra of pristine Ir(F2OC11ppy)$_3$ in THF and thin film state, and its nanocomposite film.

503 nm. The emission band at 503 nm is assigned to the emission of the iridium complex itself as located in solution. Moreover, a large redshifted emission band at 548 nm is due to the formation of intermolecular species, i.e. aggregates. For the nanocomposite film, a strong green emission at 551 nm was observed, while the intensity of the original emission at 503 nm diminished dramatically. It seems that the confinement of the Ir complex in ordered mesopores promoted the formation of aggregates. In order to examine the origin of the enhanced emission band at 551 nm, the blending method was applied to stimulate the distribution of Ir complex spatially. Ir(F2OC11ppy)$_3$ was blended with poly(methyl methacrylate) (PMMA) in different weight ratios, since PMMA is a non-emissive polymer that would not interfere with the emission behavior of Ir(F2OC11ppy)$_3$. The blended composite can be easily cast into a thin film because of the excellent film-forming properties of PMMA. Figure 6 demonstrates the PL spectra of the Ir(F2OC11ppy)$_3$/PMMA composite film with different weight ratios. A composite film comprising 10% Ir(F2OC11ppy)$_3$ and 90% PMMA showed only a major band at 500 nm, indicating the emission of the Ir complex itself. As the content of the Ir complex increases, the emission band at 550 nm dominates the PL spectrum. A large extent of aggregation is formed eventually. The PL spectrum of the composite film comprising 98% Ir(F2OC11ppy)$_3$ and 2% PMMA is quite similar to that of the nanocomposite film, implying that the Ir complex tends to aggregate inside the ordered nanopores. This observation is different from our previous report that chromophores can be segregated in nanopores formed through self-assembly [18]. One possible reason for this phenomenon is explained as follows. The Ir(F2OC11ppy)$_3$ monomer is a spherical molecule with three hydroxyl side chains. These hydrophilic hydroxy groups can react with not only the TOES moiety but also the iridium complex itself through the sol–gel process. An ordered mesostructure is formed by some iridium monomers and silica, while excess monomers would react with each other inside the nanopores. From the viewpoint of spatial distribution, a higher degree of aggregation is expected to form in those nanopores

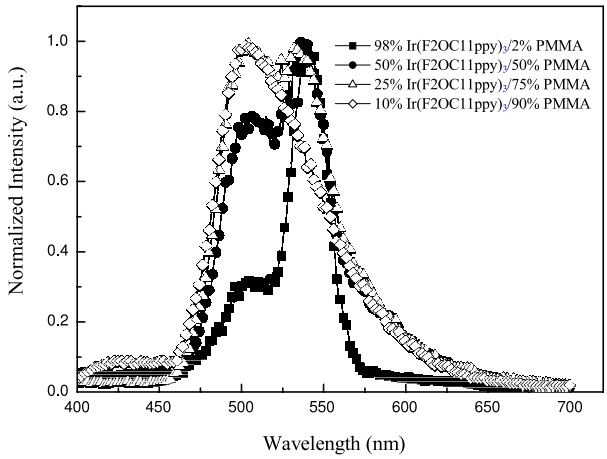

Figure 6. PL spectra of Ir(F2OC11ppy)$_3$/PMMA composite film with different weight ratios.

compared to the conventional film state. Stronger π–π intermolecular interaction consequently results in a redshift in PL emission.

The speculation was also supported by photoluminescence quantum yield (PLQY) measurements to demonstrate strong molecular interaction of the Ir(F2OC11ppy)$_3$ nanocomposite film. The PLQY of Ir(F2OC11ppy)$_3$ in THF is measured to be 62% using an integrating sphere. In going from the solution to the film state, the PLQY was decreased to 23.5%. This is normal for most organic materials by intermolecular vibronic interactions to induce a non-radiative deactivation process or by excitonic coupling, excimer formation, and excitation energy migration to the impurity traps. The PLQY of the Ir(F2OC11ppy)$_3$ nanocomposite film, however, is further reduced to 11.2%, indicating stronger intermolecular interactions in the nanocomposite film. This observation is also different from the previous result that PLQY can be improved two or three times via the sol–gel co-assembly process [9, 10]. The result also suggests that different molecular structure and modification may result in a different photophysical phenomenon during the sol–gel process. The

Table 1. Electrochemical properties of Ir(F2OC11ppy)$_3$ and CA-C11 nanocomposites.

Nanocomposite	Optical bandgap (eV)[a]	E_{ox} (eV)[b]	E_{red} (eV)[b]	HOMO (eV)[c]	LUMO (eV)[c]
mer-Ir(F2OC11ppy)$_3$	2.98 (415)	1.18	−1.80	−5.58	−2.60
CA-C11	4.00 (310)	1.50	−2.50	−5.90	−1.90

[a] The optical bandgap estimated from the onset wavelength (value in parentheses) of UV–vis absorption spectra of the nanocomposite film.
[b] The E_{ox} and E_{red} are the onset potentials of oxidation and reduction, respectively.
[c] Calculated from the empirical formulae:
$E_{(HOMO)} = -(E_{ox} + 4.40)$ (eV), $E_{(LUMO)} = -(E_{red} + 4.40)$ (eV).

number of hydrophilic groups and molecular structures should be considered overall.

3.2. Cyclic voltammetry

In this study we plan to develop a new way to fabricate phosphorescent devices via the sol–gel process, using a carbazole-based monomer CA-C11 as host material in the formed nanocomposite. The electrochemical behaviors of Ir(F2OC11ppy)$_3$/silica and CA-C11/silica nanocomposites were investigated by cyclic voltammetry (CV) (see supplementary information, figure S1 available at stacks.iop.org/Nano/20/315601). The corresponding highest-occupied molecular orbital (HOMO) and lowest-unoccupied molecular orbital (LUMO) energy levels were estimated from the onset of the redox potentials. HOMO and LUMO levels of the chromophores were calculated according to empirical formulae $E_{HOMO} = -(E_{ox} + 4.4)$ (eV) and $E_{LUMO} = -(E_{red} + 4.4)$ (eV). From the difference of the onset potentials and the optical bandgaps (E_g) calculated from the onsets of UV–vis absorption spectra, the energy levels of two nanocomposites were determined and summarized in table 1. The corresponding energy level diagram of each material is depicted in figure 7. The HOMO and LUMO levels of CA-C11 nanocomposites are −5.90 and −1.90 eV, respectively. The large bandgap of CA-C11 nanocomposites could totally cover the bandgap of the iridium complex, which means it could act as a high-efficiency charge transport material in the phosphorescent devices. On the basis of CV characteristics and the energy diagram, Ir(F2OC11ppy)$_3$ would act as a more effective trap site for electrons and holes to recombine together in the co-assembly emitting layer while CA-C11 is employed as the host, with a HOMO energy barrier of 0.3 eV and LUMO energy barrier of 0.7 eV between Ir(F2OC11ppy)$_3$ and CA-C11. In addition, the sol–gel co-assembly process brings the advantage of a good film-forming property. Moreover, the non-soluble characteristic after being cast into a thin film also provides a good opportunity to fabricate multilayer devices via the solution process, which has the potential to yield a cheaper OLED device.

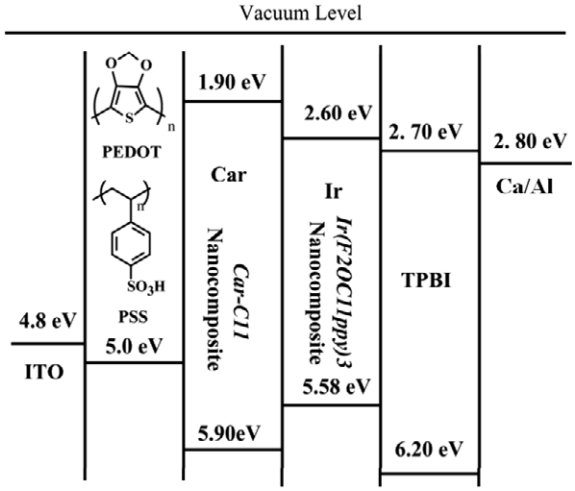

Figure 7. Schematic illustration of the energy level diagram.

3.3. Device fabrication and characterization

To evaluate the EL performance of the iridium complex in this study, two different device architectures were designed and fabricated. Device A was designed as a double-layer structure with the configuration of ITO/PEDOT:PSS(50 nm)/Ir(F2OC11ppy)$_3$:CA-C11:PBD nanocomposite (50 nm)/LiF (5 nm)/Al (100 nm). LiF was used to help the injection of electrons into the emissive layer (EML). PBD was added to facilitate the electron transport in the device. Device B was a triple-layer device with the configuration of ITO/PEDOT (50 nm)/Ir(F2OC11ppy)$_3$:CA-C11:PBD nanocomposite (50 nm)/TPBI (20 nm)/Ca (35 nm)/Al (100 nm). TPBI was inserted between EML and the cathode to act as an electron transport and hole-blocking layer. In both devices EML was composed of Ir(F2OC11ppy)$_3$, CA-C11 and PBD with a weight ratio of 1:99:20, respectively.

Figure 8(a) shows the EL spectra of device A at different bias. It emitted a sky-blue light at 9 V with CIE'1931 coordinates located at (0.19, 0.26). At higher voltage the emissive light was unchanged to the naked eye. Figures 8(b) and (c) reveal the current density–voltage and luminance–voltage characteristics of the two devices. Figure 8(d) demonstrates the efficiency–current density characteristics of the two devices. It is noted that both luminance and current density are lower for device B as compared to device A at the same voltage. The maximum efficiency of device B at low current density is thus higher than that of device A as a result of the insertion of the TPBI layer. An improvement of approx. 43% in device efficiency is observed. These values represent a fourfold enhancement in maximum luminance and a twofold enhancement in efficiency over pristine iridium complex material [19]. The incorporation of CA-C11 monomer with phosphorescent amphiphile Ir(F2OC11ppy)$_3$ to form nanocomposite films is achieved to produce a electrophosphorescent OLED device. For comparison purposes, we also fabricated a device C with the configuration of ITO/PEDOT (50 nm)/Ir(F$_2$OC11PPy)$_3$:CA-C11:PBD (50 nm)/TPBI (20 nm)/Ca (35 nm) /Al (100 nm). The EML was deposited with a thickness of 50 nm

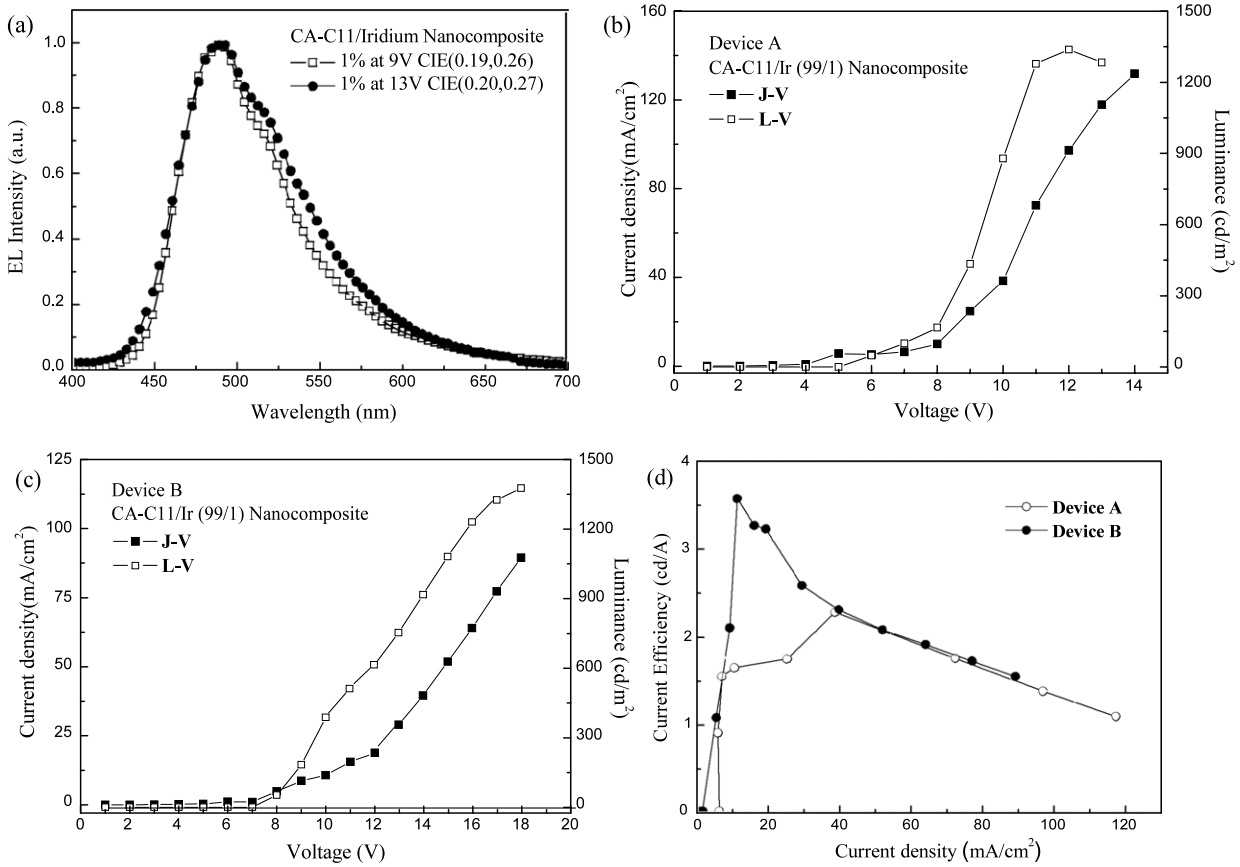

Figure 8. (a) EL spectra of device A at different bias; (b) current density–luminance–voltage (J–L–V) characteristics of device A; (c) current density–luminance–voltage (J–L–V) characteristics of device B; (d) current efficiency–current density characteristics of devices A and B.

by thermally evaporating the $Ir(F_2OC11PPy)_3$:CA-C11:PBD mixture with a weight ratio of 1:99:20. The maximum brightness and luminance of device C were 220 cd m^{-2} at 12 V and a maximum efficiency of 0.52 cd m^{-2}. The above results demonstrate that devices A and B show much better device performance than that of device C.

4. Conclusions

We demonstrate the preparation of the new phosphorescent iridium complex and its amphiphile/silica co-assembled nanocomposite film. The spatial orientation of the chromophore amphiphiles within the mesoscopic structures by sol–gel co-assembly and subsequent formation of well-ordered chromophore nanopackets in this fashion dramatically impact the photophysical properties of this material. The electrophosphorescent OLED devices were fabricated by the incorporation of a carbazole derivative CA-C11 to act as a host material in the formed nanocomposite. Multilayer devices can be achieved by a simple solution process, instead of the thermal evaporation method. The idea may have future impact in the fabrication and device performance of the nanosized OLEDs.

Acknowledgments

The authors acknowledge the financial support from the National Science Council of the Republic of China (NSC97-3114-M-009-002) and the Ministry of Education (MOE ATU Program).

References

[1] Zhang Q, Ariga K, Okabe A and Aida T 2004 *J. Am. Chem. Soc.* **126** 988
[2] Tsai C, Tam S, Lu Y and Brinker C J 2000 *J. Membr. Sci.* **169** 255
[3] Domansky K, Liu J, Wang L Q, Engelhard M H and Baskaran S 2001 *J. Mater. Res.* **16** 2810
[4] Ganschow I B M, Schulz-Ekloff G and Wohrle D 2003 *Host–Guest Systems Based on Nanoporous Crystals* (Weinheim: Wiley–VCH Verlag)
[5] Yang P D *et al* 2000 *Science* **287** 465
[6] Braun I, Ihlein G, Laeri F, Nockel J, Schulz-Ekloff G, Schulth F, Vietze U, Weiss O and Wohrle D 2000 *Appl. Phys.* B **70** 335
[7] Miller R D 1999 *Science* **286** 421
[8] Fan H, Bently R, Kathan K R, Clem P, Lu Y and Brinker C 2001 *J. Non-Cryst. Solids* **285** 79
[9] Bhongale C J and Hsu C S 2006 *Angew. Chem. Int. Edn* **45** 1404
[10] Yang C H, Bhongale C J, Liao Y M and Hsu C S 2007 *J. Mater. Chem.* **17** 243
[11] Veinot J G C and Marks T J 2005 *Acc. Chem. Res.* **38** 632
[12] Baldo M A, O'Brien D F, You Y, Shoustikov A, Sibley S, Thompson M E and Forrest S R 1998 *Nature* **395** 151
[13] Baldo M A, Lamansky S, Burrows P E, Thompson M E and Forrest S R 1999 *Appl. Phys. Lett.* **75** 4
[14] Cleave V, Yahioglu G, Le Barny P, Friend R H and Tessler N 1999 *Adv. Mater.* **11** 285

[15] Zhen H, Jiang C, Yang W, Jiang J, Huang F and Cao Y 2005 *Chem.—Eur. J.* **11** 5007
[16] Namdas E B, Ruseckas A, Samuel I D W, Lo S C and Burn P L 2005 *Appl. Phys. Lett.* **86** 091104
[17] Lo S C, Male N A H, Markham J P J, Magnennis S W, Burn P L, Salata V and Samuel I D W 2002 *Adv. Mater.* **14** 975
[18] Brinker C J, Lu Y, Sellinger A and Fan H 1999 *Adv. Mater.* **11** 579
[19] Laskar I R, Hsu S F and Chen T M 2005 *Polyhedron* **24** 189
[20] Valle K, Belleville P, Pereira F and Sanchez C 2006 *Nat. Mater.* **5** 107
[21] Rama Rao G V, Lopez G P, Bravo J, Pham H, Datye A K, Xu H and Ward T L 2002 *Adv. Mater.* **14** 1301